IEEE Access
Multidisciplinary | Rapid Review | Open Access Journal

Received September 12, 2018, accepted October 8, 2018, date of publication October 11, 2018, date of current version November 8, 2018.

Digital Object Identifier 10.1109/ACCESS.2018.2875550

Design and Fuzzy Sliding Mode Admittance Control of a Soft Wearable Exoskeleton for Elbow Rehabilitation

QINGCONG WU[1], (Member, IEEE), XINGSONG WANG[2], BAI CHEN[1], AND HONGTAO WU[1,3]

[1]College of Mechanical and Electrical Engineering, Nanjing University of Aeronautics and Astronautics, Nanjing 210016, China
[2]College of Mechanical Engineering, Southeast University, Nanjing 211189, China
[3]State Key Laboratory of Robotics and System, Harbin Institute of Technology, Harbin 150001, China

Corresponding author: Qingcong Wu (wuqc@nuaa.edu.cn)

This work was supported in part by the National Natural Science Foundation of China under Grant 51705240, in part by the Natural Science Foundation of Jiangsu Province of China under Grant BK20170783, in part by the Aeronautical Science Foundation of China under Grant 2017ZC52037, and in part by the State Key Laboratory of Robotics and System (HIT) under Grant SKLRS-2018-KF-10.

ABSTRACT Exoskeletons composed of rigid frames and joints have been widely implemented in rehabilitation application. However, the rigid mechanical structure introduces many problems, such as heavy weight, large inertia, and joint misalignment. To overcome these undesirable inherent disadvantages of rigid exoskeletons, the innovative contributions of this paper are to investigate the design and fuzzy sliding mode admittance (FSMCA) control of a soft wearable exoskeleton with compliance tendon-sheath actuation (CTSA) for multi-mode elbow rehabilitation training. The CTSA system is developed on the base of the Hill-based muscle model to imitate the working characteristics of human muscle and improve the compliance and coordination of human–robot cooperation. The FSMCA controller is capable of providing patient-passive and patient-active therapies under different training intensities and encouraging the active participation of the patients with various weakness levels. Further experimental investigations, including the trajectory tracking experiments with/without admittance regulation, the step response experiments with disturbance, the frequency response experiments, and the patient-active training experiments, are carried out by three healthy volunteers. Experimental results demonstrate the effectiveness of the proposed FSMCA control scheme in achieving high control accuracy and favorable frequency response characteristic. Besides, the training intensity can be qualitatively adjusted via appropriate admittance parameters.

INDEX TERMS Soft wearable exoskeleton, elbow rehabilitation, fuzzy sliding mode admittance control, patient-passive training, patient-active training.

I. INTRODUCTION

Stroke is a serious neurological disease causing physical disability and cognitive impairment. The statistical results from the World Heathy Organization indicate that there are more than 15 million people annually suffering from the effect of stroke [1]. And about three quarters of the stroke patients survive and need prolonged physical treatment to recover motor functions in activities of daily living (ADL). Clinical researches on the neurological rehabilitation training show that repetitive motions have positive effects on improving the muscle strength and movement coordination of affected limb and promoting the plasticity of brain. Traditionally, the physiotherapists need to manually provide one-on-one treatment to the disabled patients based on their own therapeutic experience, like passive movement guidance and progressive resistive training. However, the conventional approaches have many limitations, such as high labor intensity, limited treatment outcome, long time consumption, subjective therapy evaluation and high expense [2].

Compared with the traditional manually therapy, the robot-assisted therapy is more suitable for the rehabilitation training after stroke, as it can deliver high-intensity training and guarantee repetitive consistency. Moreover, the training data and therapy effectiveness of patient can be precisely recorded via the integrated sensing system, which enable diagnostic measurement and quantitative optimization of the rehabilitation schemes [3]. In recent decades, many kinds of upper limb rehabilitation exoskeletons, which imitate the human arm skeleton and operate in parallel with the affected limb, have been developed for the treatment of disabled patients.

For example, Otten *et al*. developed a hydraulically powered exoskeleton, named LIMPACT, to identify the reflex properties of stroke survivors and perform upper limb rehabilitation training [4]. Keller *et al*. proposed an upper limb exoskeleton with audiovisual therapy interface, called ChARMin, for the pediatric arm rehabilitation of children and adolescents [5]. ETS-MARSE is a redundant exoskeleton with seven degrees of freedom for superior extremity training [6]. Besides, many other exoskeletons have been developed for arm rehabilitation, such as RUPERT [7], HES [8], ULEL [9], and ArmeoPower [10]. These previous exoskeletons are typically composed of rigid frames to transmit force to the ground or apply driving torques to human joints. However, the rigid nature presents several practical challenges to the rehabilitation application, such as heavy body weight, large structure dimension and high power consumption. To reduce the body weight of exoskeleton, many flexible transmission systems have been adopted to separate the actuator from the exoskeleton, such as tendon-sheath system [11], [12], cable-driven system [13]–[15], and webbing ribbon [16]. Another serious drawback of rigid exoskeleton is that the rigid links may impose undesirable interaction force on the affected limb if the biological joints and robot joints are not completely aligned. Various auxiliary mechanisms have been integrated into exoskeletons to eliminate the hyperstaticity resulting from misalignments, such as redundant joint [17], shoulder mechanism with misaligned axis [18], self-aligning platform [19], slider crank mechanisms [20], and double-shelled links [21]. Unfortunately, these solutions lead to more complex mechanism structure and lower system reliability.

Taking the aforementioned disadvantages of the rigid exoskeletons into account, more and more researchers focus on developing the soft exoskeleton with lightweight and low inertias. The soft exoskeleton uses the clothing-like textiles to interface with the body of wearer, and the compressive force directly acts on the human skeleton during rehabilitation training. Furthermore, since there are no rigid joints and links in the wearable robot system, the joint-misalignment problem can be effectively eliminated. At present, most of the existing soft exoskeletons are focused on the assistance of lower limb [17], [22]–[25]. Only a few of soft upper limb exoskeletons have been proposed. O'Neill *et al*. developed a wearable soft robot driven by textile pneumatic actuators for shoulder assistance [26]. An upper body soft exosuit called FlyJacket is develope by Rognon *et al*. for the teleoperation of an immersive drone [27]. Copaci *et al*. proposed a soft elbow exoskeleton based on shape memory alloy (SMA) wire actuators. The major limitation is that the control accuracy and driving force of SMA are difficult to guarantee [28].

The control strategies applied in the rehabilitation robots directly determine the effectiveness of robot-assisted therapy. The existing control schemes for rehabilitation training can be basically divided into passive mode controller and active mode controller. Many fuzzy-based controllers have been developed to compensate unknown disturbances and improve the position control accuracy of passive mode training [29]–[32]. The disadvantages of passive mode training is the lack of active participation of patient. Surface electromyography (sEMG) signals [33]–[35] and electroencephalogram (EEG) signals [36], [37] have been used in the exoskeleton to detect human motion intention and provide active mode training. However, the adjustment of rehabilitation training intensity is unrealizable for these control strategies.

Taking the above issues into account, the contribution of this paper is to develop a new soft wearable exoskeleton for the elbow flexion/extension rehabilitation training of disabled patients. Besides, a novelty compliant-tendon-sheath actuator (CTSA) is developed based on the Hill-based muscle-tendon model to imitate the morphology of biological muscle-tendon tissue. The CTSA is integrated into the soft robot to provide active compliant assistance and ensure interaction safety. In order to allow the disabled individuals perform passive and active training based on their weakness levels and treatment programs, a fuzzy sliding mode admittance (FSMCA) control strategy is proposed, which can adjust training intensity and encourage the active participation of patients. Finally, the effectiveness of the developed soft exoskeleton and FSMCA control scheme are evaluated via two types of experiments with three healthy volunteers.

II. DESIGN OF THE SOFT ELBOW EXOSKELETON

A. HARDWARE DESCRIPTION

A diagram of the overall structure of the soft exoskeleton worn on the left and right elbows is shown in Fig. 1. It is designed to assist the wearer suffering from muscle weakness perform elbow flexion and extension rehabilitation training. The overall system is mainly consisted of two compliant tendon-sheath actuator units, four tendon-sheath units, four sheath supports, four anchor points, two guidance mechanisms, and two soft wrap units combined with Velcro straps. The actuator units are located on the backside of waist via belts and braces. The diving forces from the actuation system can be transmitted to the soft exoskeleton via tendon-sheath units. The routing of the tendon-sheath is designed to pass approximately through the biological joint center of shoulder to avoid undesirable torque acting on the non-targeted joint. The sheath supports mounted on upside of soft wrap are used to sustain the pushing force from outer sheathes, while the anchor points mounted on the bottom of soft wrap can transmit the pulling force from the tendon to the human forearm. The location and winding diameter of Velcro traps can be adjusted to adapt to the subjects with body heights ranging from 1.5 m to 2 m. The actuation unit is capable of providing driving moment to the elbow joint, as the pulling forces from the tendons deviate from the rotation center of elbow. To ensure the fixation of tendons to human body, the stiffness of the selected strap is relatively large to reduce the elastic deformation under external pulling forces. Besides, the soft wraps worn on elbow are moderately tight, and that facilitates to distribute the load applied on the human body, adjust tendon length, and maximize comfort. The guidance

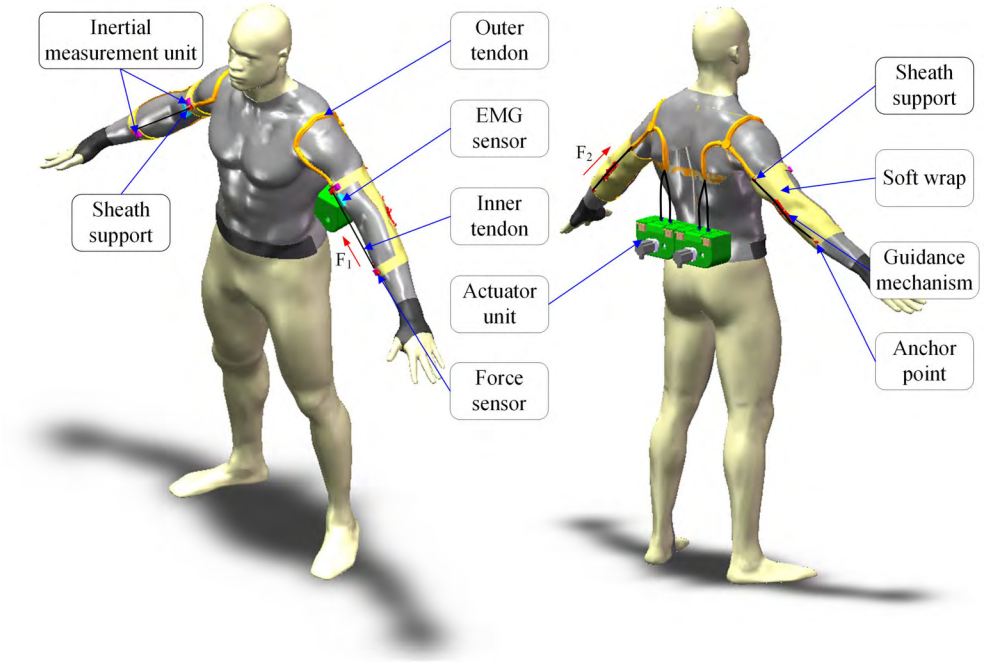

FIGURE 1. Overall structure of the developed soft elbow rehabilitation exoskeleton.

mechanism with leading sheaves is located on the backside of the elbow. It can adjust the transmission direction of tendon in accordance with the elbow configuration and protect the human body from the shear force from tendon. The total weight and volume of the soft exoskeleton (including the actuator) are about 2.37 kg and 1.65×10^{-2} m^3.

The inertial measurement units (IMU), force sensors, and sEMG sensors are integrated into the soft therapeutic system to acquire the real-time data of patient and robot in training. Two nine-axes IMU sensors (TELESKY, MPU9250) are located on the upper arm and forearm of wearer to measure the configuration of each elbow. The miniature force sensor (KINGNO, JLBS-MD) is mounted between the distal end of tendon and corresponding anchor point to detect the pulling force from actuator. The sEMG signals from the bicipital muscle of wearer are obtained via the sEMG signal measurement system (Sichiray, Sunlephant-6 EMG System), which provide information on the scale of muscular power and activation pattern. Considering the safety during training, two mechanical end stoppers are mounted on the pulleys to limit the range of motion of exoskeleton and protect the wearer from excessive flexion and extension. Besides, the electrical watchdog and monitoring program are applied to observe the actual motor speeds, motor currents, driving torques and pulling forces and supervise system functionality. Two dead-man buttons can be pressed by the physiotherapist and patient immediately to break the power supply in the case of emergency.

B. COMPLIANT TENDON-SHEATH ACTUATION

The tendon-sheath actuation is a flexible transmission system consisting of a slender helical tension spring as the outer sheath and a steel wire rope as the inner tendon. It is capable of providing remote power transmission through the narrow tortuous space, and thus has been widely applied in designing the robots with soft structure and small size, such as surgical robots, rescue robots, and soft robots [38], [39]. Inspired by the working principle of antagonistic muscles and tendon-sheath transmission, a compliant tendon-sheath actuation system is developed on the base of the Hill-based muscle-tendon model to imitate the operating properties of human muscle and, furthermore, improve the coordination and performance of human-robot cooperation, as shown in Fig. 2. The Hill-based muscle-tendon model has been commonly utilized to describe the mechanical characteristics of muscle [40]. It consists of a contraction element (CE) generating the active driving force, a series elastic element (SE) representing the

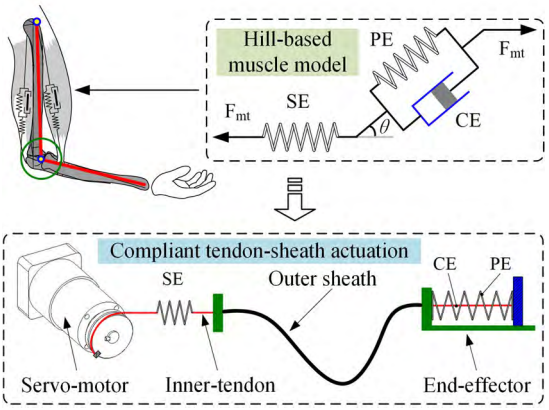

FIGURE 2. Schematics of the compliant tendon-sheath actuation system developed based on Hill-based muscle-tendon model.

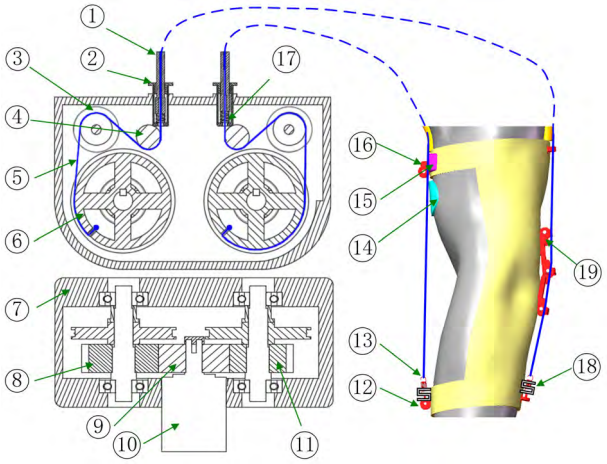

FIGURE 3. Schematics of the compliant tendon-sheath actuator unit (1-Outer sheath; 2-Pretension thread tube; 3-Tension sensors; 4-Guiding wheel; 5-Inner tendon; 6-Pulley; 7-Shell frame; 8-Large driven gear; 9-Driving gear; 10-Servo motor; 11-Small driven gear; 12-Anchor point; 13-Series tension spring; 14-SEMG sensor; 15-IMU sensor; 16-Sheath support; 17-Parallel pressure spring; 18-Force sensor; 19-Guidance mechanism.

intrinsic elasticity of myofilaments, and a parallel elastic element (PE) representing the passive force of tissues [41]. The compliant tendon-sheath actuation is designed according to this three-element model. More specifically, a tension spring is connected in series with the inner tendon to work as the SE; a pressure spring is connected in parallel with the inner tendon to work as the CE; and the tendon-sheath system works as the PE to provide contraction force. The driving force generated in the proximal servo motor can be transmitted to the distal end-effector through tendon-sheath transmission system with arbitrary configuration, and the deformations of tension spring and pressure spring help to increase the compliance of actuator. The parameters of each spring should be determined in accordance with the parameters of Hill-based muscle-tendon model. The proposed compliant tendon-sheath actuation system has light weight, small dimension, flexible structure and similar properties as the human muscle. Therefore, it is applicable to the design of soft rehabilitation elbow exoskeleton.

The compliant tendon-sheath actuator unit used for the actuation of each elbow has been designed and shown in Fig. 3. A servo AC motor (SGM7G, YASKAWA Inc.) coupled to a planetary gear reducer (reduction of 40:1) is mounted on the backside of shell frame to provide bidirectional driving forces for the elbow flexion and extension. A driving gear is attached to the output shaft of reducer and engages with a large driven gear and a small driven gear with different gear ratios, respectively. Two pulleys with a diameter of 80 mm are connected to each driven gear via shafts and keys. The proximal ends of two inner tendons, made from stainless steel wires with a diameter of 1 mm, are attached to the pulleys at the actuation side. The distal ends of inner tendons firstly pass round the tension sensors (TAMEG, JZHL-1) and guiding wheels and, after that, thread the outer

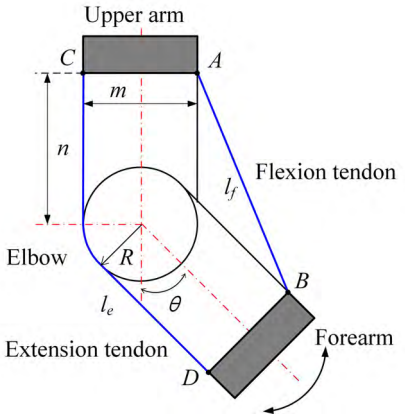

FIGURE 4. Schematics of the tendons routing on the elbow of wearer.

sheathes and are fastened to the soft elbow exoskeleton. The outer sheathes are tightly wound springs made from 0.6 mm alloy steel and have an inner diameter of 1.2 mm. The maximum torque generated by the compliant actuator is about 8.23 N · m.

With the aim of eliminating the slacking problem due to the elastic deformation of tendon, the tendon length and system pretension can be adjusted by tightening or loosening the pretension thread tubes installed on the top of shell frame. Two pressure springs are packaged into the pretension thread tubes in parallel with the inner tendons to work as the CE of muscle model. On the other hand, two tension springs are connected in series with the distal ends of inner tendons to work as the SE of muscle model. The proximal ends of sheathes are inserted into the pretension thread tubes to exert pushing force on the pressure springs, while the distal ends are fixed to the sheath supports. With the actuation of servo motor, the rotation of pulleys can be transformed into the linear movement of tendons and, finally, actuate the biological elbow joints with the soft exoskeleton.

C. ANALYSIS OF TENDON ROUTING

The compliant tendon-sheath transmission units in both sides of joint are pulled in different directions to perform elbow flexion and extension. In order to guarantee the movement coordination of the two tendons attached to the elbow, the transmission ratios of the diving gear and driven gears should be determined based on the relationship between tendon displacement and elbow joint angle. The schematics of the tendons routing on the elbow of wearer can be simplified and shown in Fig. 4. The elbow is actuated by the flexion tendon and extension tendon in agonist-antagonist configuration. Points A and C denote the sheath supports located on the upper limb. Points B and D represent the anchor points located on the forearm. The length of flexion tendon between points A and B is denoted as l_f, while the length of extension tendon between points C and D is denoted as l_e. The elbow joint angle is defined as θ, and the radius of the elbow joint is denoted as R. The elbow is completely extended when $\theta = 0$. The range of movement of the soft exoskeleton is limited

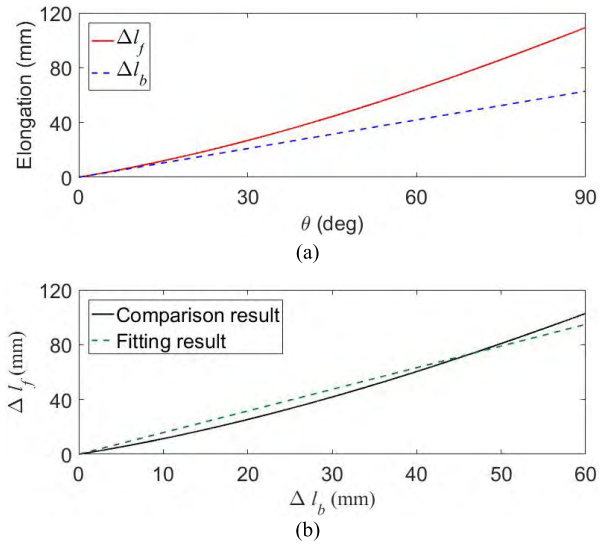

FIGURE 5. The elongations of different tendons as the elbow joint angle change from 0° to 90°. (a) The length variations of the flexion tendon and extension tendon. (b) The comparison result and fitting result of the elongation values.

via mechanical stops and monitoring program. The maximum elbow joint angle is 110°. The widths of the upper arm and forearm are all equal to m. The distances from the elbow joint center to the intersecting surfaces, where the sheath supports and anchor points are mounted on, are all equal to n.

Based on the geometrical relations presented in Fig. 4, the length variations of the tendons, which change with the elbow joint angle, can be calculated as follows:

$$\Delta l_f(\theta) = 2n - \sqrt{m^2 + 4n^2}\cos\left[\arctan(\frac{m}{2n}) + \frac{\theta}{2}\right] \quad (1)$$

$$\Delta l_e(\theta) = R\theta \quad (2)$$

where $\Delta l_f(\theta)$ and $\Delta l_e(\theta)$ denote the elongation of flexion tendon and extension tendon, respectively.

From (1) and (2), the elongation of flexion tendon can be expressed as a nonlinear function of elbow joint angle. According to the anthropometry in movement in biomechatronics [42] and the established virtual prototype model of soft exoskeleton, the following parameters are adopted to analyze the relationship between $\Delta l_f(\theta)$ and $\Delta l_e(\theta)$: m = 80 mm, $R = 40$ mm, $n = 90$ mm, $\theta = [0° - 90°]$. Thus, the resulting elongations of flexion tendon and extension tendon can be calculated and shown in Fig. 5 (a). It can be clearly observed that the elongation of flexion tendon is larger than that of the extension tendon. The solid line shown in Fig. 5(b) gives the comparison results of the elongations of different tendons. As can be found, the elongation of flexion tendon is approximately proportional to that of the extension tendon. Therefore, a line passing through the ordinate origin can fit the comparison results. The dashed line shown in Fig. 5(b) give the fitting result that minimizes the root mean squared error (RMSE) between the actual and fitting elongations of flexion tendon when $\Delta l_e(\theta)$ varies from 0 mm to 60 mm. The obtained minimum RMSE is about 4.8 mm when the slope

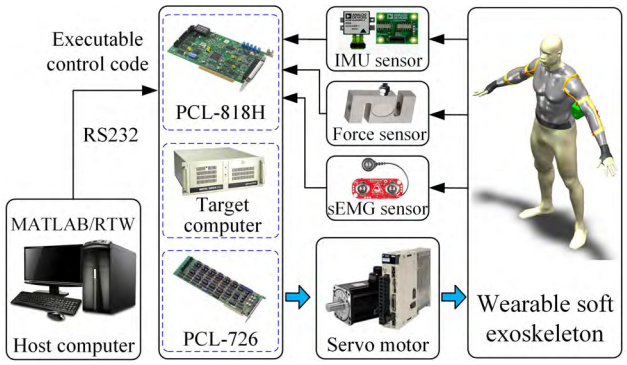

FIGURE 6. The hardware architecture diagram of Matlab/Real-Time-Workshop/xPC control system.

of the fitting line is set to 1.6. Thus, to avoid the undesirable stain on the elbow that comes from the insufficient release of different tendons, the transmission ratio between the driving gear and large driven gear should be set as 1.6 times the transmission ratio between the driving gear and small driven gear. Meanwhile, the series springs and parallel springs of actuation and the soft wrap can compensate the residual elongation difference and improve interactive coordination.

D. REAL-TIME CONTROL SYSTEM

The real-time control system of the proposed soft therapeutic exoskeleton is established in the Matlab/xPC environment (Mathworks Inc.) with a closed-loop hierarchical architecture, as shown in Fig. 6. The control system is set to work in the dual-machine collaborative mode. It is mainly composed of a host control layer and a target control layer which are established in two industrial personal computers (IPC-610H, Advantech Inc.) respectively. The host controller is in charge of generating the Simulink control models based on the predefined control strategy. And then, the control models can be translated into the executable control codes and transmitted to the real-time target controller through RS232 serial port. The target controller is installed with a real-time-workshop kernel and capable of executing the embedded algorithms and controlling the exoskeleton operation. The feedback analog signals from the IMU sensor, force sensors and sEMG sensors are acquired by two high-precision analog-to-digital (A/D) converters (PCL-818H, Advantech Inc.) inserted into the industry standard architecture (ISA) slots of target computer. A third order low-pass Bessel filter with a cut-off frequency of 40 rad/s is utilized to filter the acquired signals and minimize the readout noise. The envelope of the sEMG signals can be obtained after the signals were full-wave rectified by a moving average window of 100 ms. Besides, two digital-to-analog (D/A) cards (PCL-726, Advantech Inc.) with an analog output resolution of 12 bits are installed in the target computer. The analogue channels of D/A cards can transform the digital control commands, generated in the real-time target computer, into analog output signals and regulate the running of servo motors. The sampling rates for the host and target control layers are all set to 1 kHz.

III. CONTROL OF THE SOFT ELBOW EXOSKELETON

A. DYNAMIC MODELING

The wearable soft elbow exoskeleton is a typical human-robot interaction system, thus the dynamic modeling of the overall system should takes into consideration both the human joint and soft exoskeleton. Assuming that the elbow movement is constrained to the sagittal plane. According to the existing literatures [43] and the schematics of elbow illustrated in Fig. 4, the dynamic model can be established by utilizing the Lagrange formulation, as shown follow:

$$\tau+\tau_h=(J_h+J_{ex})\ddot{\theta}+V_h\dot{\theta}+g(m_hL_h+m_{ex}L_{ex})[1-\cos(\theta)] + f_h\text{sign}(\dot{\theta})+F_t+D_u \quad (3)$$

Here, J_h and m_h denote the inertia and mass of the human forearm; J_{ex} and m_{ex} represent the inertia and mass of the wearable components of exoskeleton, including the soft wrap, force sensors, springs, and so on; V_h is the viscous damping coefficients of elbow joint; L_h and L_{ex} denote the distances of from the center of mass of forearm and exoskeleton to the elbow joint, respectively; g represents the gravitation vector; f_h denotes the solid friction coefficients of elbow joint;F_t is the system friction from the tendon-sheath transmission system; D_u is the lumped effects of uncertainties including external disturbances and modeling errors; τ represents the driving torque from the servo motor; τ_h is the joint torque of elbow produced via the contractions of antagonist muscles.

According the torque transmission model of tendon-sheath system proposed in our previous study [38], the transmission relationship between the driving torque from servo motor and the output torque of tendon-sheath system can be shown as follow:

$$\tau=\frac{\tau_t r}{R}+\text{sign}(\dot{\theta})2Tr\lambda\mu \quad (4)$$

where τ_t represents the output torque of tendon-sheath system; r denotes the radius of the pulleys in actuator unit; T and λ denote the pretension value and total bending angle of the tendon-sheath transmission system; μ represents the Coulomb friction coefficient between the inner tendon and outer sheath. In the developed soft exoskeleton prototype, the pulley radius is set to be equal to the radius of elbow, thus the tendon-sheath friction can be obtained from (4), as shown follow:

$$F_t=\tau-\tau_t=\text{sign}(\dot{\theta})2Tr\lambda\mu \quad (5)$$

The predicted elbow joint torque can be estimated via the sEMG signals from the bicipital muscle using the linear proportional model developed by Ao *et al.* [44], as shown follow:

$$\tau_h=GT_{MIVE}N_{EMG} \quad (6)$$

where G reflects the assistance gain for sEMG to torque conversion; T_{MIVE} is the maximum torque during isometric voluntary extension trials at 90° elbow flexion angle; N_{EMG} denotes the processed sEMG signals using the maximum recorded data and normalized to the range from 0 to 1.

Then, inserting (4), (5) and (6) into (3) gives the overall dynamic model of the human-robot interaction system, i.e.,

$$\tau=(J_h+J_{ex})\ddot{\theta}+V_h\dot{\theta}+g(m_hL_h+m_{ex}L_{ex})[1-\cos(\theta)] + \text{sign}(\dot{\theta})(f_h+2Tr\lambda\mu_t)+D_u-GT_{MIVE}N_{EMG} \quad (7)$$

B. PATIENT-ACTIVE ADMITTANCE CONTROL

The effectiveness of the robot-assisted training therapy is directly depended on the control strategies applied to the therapeutic robot system. The robot controllers should be determined according to the hemiplegia degree and rehabilitation progress of the disabled patients. The traditional control schemes can be basically divided into two categories to indicate the involvement of subjects in rehabilitation training: the patient-passive mode control scheme and the patient-active mode control scheme [45]. The patient-passive training is suitable for the patients completely paralyzed without any muscle contraction at the early stage of therapy. The therapeutic robots assist the impaired limbs passively conduct repetitive training along desired reference trajectory with small tracking errors. On the other side, if the patients have recovered partial of motor capability, the patient-active training is capable of integrating the active participation and motion intention of patients into the rehabilitation training, which benefits to the improvement of treatment efficiency.

With the aim of realizing both the patient-passive mode training and patient-active mode training via the proposed soft elbow exoskeleton, an admittance control strategy with a fuzzy sliding mode controller (FSMC) as the inner position control loop is developed to regulate the robot configuration and human-robot interaction force during training.

According to the geometric relationships between tendons and elbow shown in Fig. 4, the interaction torque acting on the elbow can by computed via the pulling forces measured by the force sensors as follow:

$$\tau_{elbow}=F_1\sin\left[\frac{\theta}{2}+\arctan(\frac{m}{2n})\right]\sqrt{n^2+\frac{1}{4}m^2}-F_2R \quad (8)$$

where F_1 and F_2 represent the pulling force from the flexion tendon and extension tendon, respectively.

The torque errors $\Delta\tau$ between the desired interaction torques τ_d and the actual interaction torque τ_{elbow} can be transmitted into the an admittance filter to calculate the value of joint angle regulation, $\Delta\tilde{\theta}$. The desired admittance characteristic describing the relationship between interaction torque and elbow joint angle can be shown as:

$$\Delta\tilde{\theta}=(\tau_{elbow}-\tau_d)\cdot\delta_F=\Delta\tau\cdot\delta_F \quad (9)$$

where

$$\delta_F=\frac{1}{M_ds^2+B_ds+K_d}$$

Here, δ_F represents the admittance value of system; M_d, B_d, and K_d denote the inertial gain, damping gain, and stiffness gain of the admittance filter.

Thus, we can get

$$\tau_d = \tau_{elbow} - \Delta\tilde{\theta}\left[M_d s^2 + B_d s + K_d\right] \tag{10}$$

From (10), it can be found that, for the same joint angle regulation, the increase of the admittance value leads to less error between the actual and desired interaction torque. By selecting the appropriate admittance parameters, the therapists can modulate the compliance of human-robot interaction and training intensity based on the practical recovery status of patients and the results of rehabilitation evaluation.

The actual joint angle error of elbow exoskeleton is defined as:

$$\Delta\theta = \theta - \theta_d \tag{11}$$

where θ_d and $\Delta\theta$ represents the desired elbow joint angle and tracking error, respectively.

Then, the admittance error ξ is defined as the difference between joint angle error and calculated joint angle regulation and can be expressed as follow:

$$\xi = \Delta\tilde{\theta} - \Delta\theta = (\tau_{elbow} - \tau_d)\cdot\delta_F + \theta_d - \theta \tag{12}$$

According to (7), the dynamic model of the human-robot system can be rewritten as:

$$\ddot{\theta} = (J_h + J_{ex})^{-1}\left[\tau - V_h\dot{\theta} - G - F_f - D_u + GT_{MIVE}N_{EMG}\right] \tag{13}$$

where

$$G = g(m_h L_h + m_{ex}L_{ex})[1 - \cos(\theta)]$$
$$F_f = \text{sign}(\dot{\theta})(f_h + 2Tr\lambda\mu_t)$$

The switching function of the sliding surface of inner FSMC-based position controller is defined via the admittance error and expressed as follow:

$$S(t) = \eta\xi + \dot{\xi} \tag{14}$$

where η denotes a positive constant of proportional gain.

The deviation of the sliding variable can be expressed as:

$$\dot{S}(t) = \eta\dot{\xi} + \ddot{\xi} \tag{15}$$

Then, inserting (12) and (13) into (15), the following equation can be obtained:

$$\begin{aligned}\dot{S}(t) &= \eta\dot{\xi} + (\ddot{\tau}_{elbow} - \ddot{\tau}_d)\cdot\delta_F + \ddot{\theta}_d - \ddot{\theta} \\ &= \eta\dot{\xi} + (\ddot{\tau}_{elbow} - \ddot{\tau}_d)\cdot\delta_F + \ddot{\theta}_d \\ &\quad - (J_h + J_{ex})^{-1}\left[\tau - V_h\dot{\theta} - G - F_f - D_u\right. \\ &\quad \left. + GT_{MIVE}N_{EMG}\right]\end{aligned} \tag{16}$$

The control input of the sliding mode controller (SMC) mainly consists of two terms, i.e., the equivalent control term and the hitting control term [46]. Totally, the general form of SMC algorithm can be expressed as:

$$u = u_{eq} + u_{hit} \tag{17}$$

Here, the equivalent control term u_{eq}, which attracts the system states to desired position and determines the system dynamic property along sliding surface, can be derived as the solution of $\dot{S} = 0$ excluding the lumped effects of uncertainties, i.e., $D_u = 0$. Therefore, according to (16), we can obtain:

$$\begin{aligned}u_{eq} = (J_h + J_{ex})\left[\eta\dot{\xi} + (\ddot{\tau}_{elbow} - \ddot{\tau}_d)\cdot\delta_F + \ddot{\theta}_d\right] \\ + V_h\dot{\theta} + G + F_f - GT_{MIVE}N_{EMG}\end{aligned} \tag{18}$$

Nevertheless, the equivalent control term cannot guarantee the control performance with undesired external disturbance and the variation of system parameters. Thus, the hitting control term u_{hit} should be applied to keep the system state lying on the sliding surface and eliminate the influences of perturbations.

It is well known that the discontinuous sign function has been widely used as the hitting control term of SMC to guarantee the system stability with uncertainties [46]. However, the serious chattering problem caused by the sign function may leads to high frequency unmodeled dynamics and poor control performance. Therefore, a fuzzy logic control strategy is developed as the hitting control term to mitigate the chattering phenomenon in our study.

The fuzzy hitting control term with the normalized sliding variable $S(t)$ as input linguistic variable can be expressed as follow:

$$u_{hit} = \text{FC}\,(S(t)) \tag{19}$$

Here, FC$(\cdot)$ is a single-input single-output nonlinear fuzzy control law developed using the Mamdani fuzzy inference algorithm [47]. In the process of fuzzification, the membership functions of the fuzzy input variable are scaled and decomposed into three trigonometry/trapezoidal fuzzy partitions, which are expressed as N (Negative), Z (Zero) and P (Positive), as illustrated in Fig. 7. Besides, the membership functions of the fuzzy output variable are divided into three subsets as NE (Negative Effort), ZE (Zero Effort) and PE (Positive Effort), as illustrated in Fig. 8. Then, the linguistic fuzzy rules are extracted to determine the input-output relationship of fuzzy logic inference mechanism. Each combination of input variable value and corresponding input membership function activates one hitting control action based on the fuzzy IF-THEN rules predefined as follows:

- Fuzzy rule 1: If $S(t)$ is N, then u_{hit} is NE;
- Fuzzy rule 2: If $S(t)$ is Z, then u_{hit} is ZE;
- Fuzzy rule 3: If $S(t)$ is P, then u_{hit} is PE.

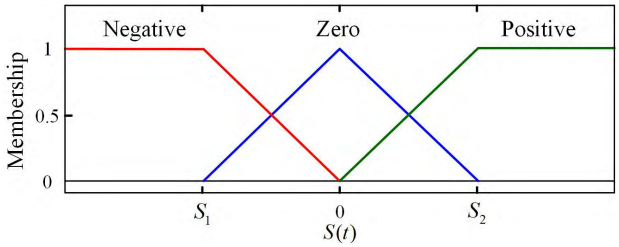

FIGURE 7. The input membership function for $S(t)$.

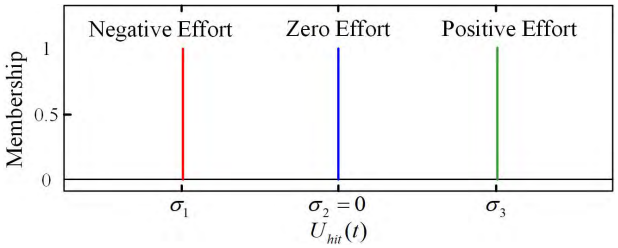

FIGURE 8. The output membership function for $U_{hit}(t)$.

For the fuzzy defuzzification operation, the center-of-gravity defuzzification process is selected to calculate the output variable of fuzzy logic inference mechanism. This approach can achieve high control sensitivity to the input variation and efficient calculation process. Then, the fuzzy hitting control law can be obtained as follow:

$$u_{hit} = \frac{\Sigma_{j=1}^{3}\sigma_j A(\sigma_j)}{\Sigma_{j=1}^{3}A(\sigma_j)} = \sigma_1 A(\sigma_1) + \sigma_2 A(\sigma_2) + \sigma_3 A(\sigma_3) \quad (20)$$

where $0 \leq \mathrm{A}(\sigma_j) \leq 1$ denotes the firing strength of rule j, and the sum of the firing strength of each rule satisfies the following equation: $\mathrm{A}(\sigma_1) + \mathrm{A}(\sigma_2) + \mathrm{A}(\sigma_3) = 1$. $\sigma_1 = -\sigma$, $\sigma_2 = 0$, and $\sigma_3 = \sigma$ represent the center of output membership function NE, ZE, and PE. Here, σ denotes a predefined positive constant. Thus, the real-time adjustment of hitting control law can be realized based on the variation of sliding variable.

From the proposed membership functions and fuzzy rules, the following four situations can be summarized:

a) If $S_2 < S(t)$, then only rule 3 is activated. We can get: $A(\sigma_3) = 1, A(\sigma_1) = A(\sigma_2) = 0, U_{hit}(t) = \sigma_3 A(\sigma_3) = \sigma$.
b) If $0 < S(t) \leq S_2$, then both rule 2 and rule 3 are activated. We can get: $0 < A(\sigma_2) \leq 1, 0 < A(\sigma_3) \leq 1, A(\sigma_1) = 0, U_{hit}(t) = \sigma_2 A(\sigma_2) + \sigma_3 A(\sigma_3) = \sigma A(\sigma_3)$.
c) If $S_1 < S(t) \leq 0$, then both rule 1 and rule 2 are activated. We can get: $A(\sigma_3) = 0, 0 < A(\sigma_1) \leq 1, 0 < A(\sigma_2) \leq 1, U_{hit}(t) = \sigma_1 A(\sigma_1) + \sigma_2 A(\sigma_2) = -\sigma A(\sigma_1)$.
d) If $S_1 > S(t)$, then only rule 1 is activated. We can get: $A(\sigma_2) = A(\sigma_3) = 0, A(\sigma_1) = 1, U_{hit}(t) = \sigma_1 A(\sigma_1) = -\sigma$.

Then, according to the analysis results of the above four possible situations, it can be easily found that:

$$S(t)[A(\sigma_3) - A(\sigma_1)] = |S(t)| \cdot |A(\sigma_3) - A(\sigma_1)| \geq 0 \quad (21)$$

Finally, by combing (17)-(20) and considering the above four different situations, we can get the complete FSMCA control law, i.e.,

$$u = (J_h + J_{ex})\left[\eta\dot{\xi} + (\ddot{\tau}_{elbow} - \ddot{\tau}_d)\cdot\delta_F + \ddot{\theta}_d\right] + V_h\dot{\theta} + G + F_f - GT_{MIVE}N_{EMG} + \sigma\left[A(\sigma_3) - A(\sigma_1)\right] \quad (22)$$

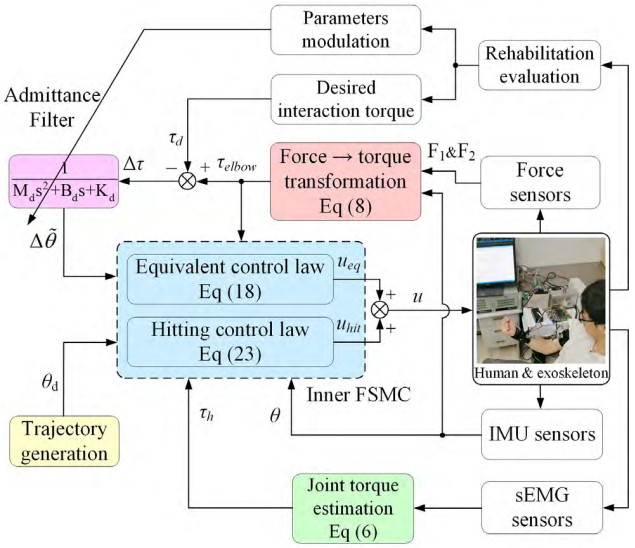

FIGURE 9. The overall block diagram of the FSMC-based admittance control strategy.

The overall block diagram describing the proposed control scheme is presented in Fig. 9. The system stability with the proposed control strategy is analyzed via the Lyapunov stability theory. Define a positive-definite Lyapunov function candidate as follow:

$$V(t) = \frac{S^2(t)}{2} \quad (23)$$

Differentiating (23) with respect to time and using (16), we can get that:

$$\dot{V}(t) = S(t)\dot{S}(t) = S(t)\begin{bmatrix}\eta\dot{\xi} + (\ddot{\tau}_{elbow} - \ddot{\tau}_d)\cdot\delta_F + \ddot{\theta}_d - \\ (J_h + J_{ex})^{-1}(\tau - V_h\dot{\theta} - G - F_f - D_u \\ + GT_{MIVE}N_{EMG})\end{bmatrix} \quad (24)$$

Then, inserting (16) into (24), we can get that (25), as shown at the bottom of this page.

From (21), (25) can be rewritten as follow:

$$\begin{aligned}\dot{V}(t) &= -(J_h + J_{ex})^{-1}\sigma S(t)\left[A(\sigma_3) - A(\sigma_1)\right] \\ &\quad + (J_h + J_{ex})^{-1}S(t)D_u \\ &= -(J_h + J_{ex})^{-1}\sigma\,|S(t)|\,|A(\sigma_3) - A(\sigma_1)| \\ &\quad + (J_h + J_{ex})^{-1}S(t)D_u\end{aligned}$$

$$\dot{V}(t) = S(t)\left\{\begin{array}{l}\eta\dot{\xi} + (\ddot{\tau}_{elbow} - \ddot{\tau}_d)\cdot\delta_F + \ddot{\theta}_d - \\ (J_h + J_{ex})^{-1}\left\{\begin{array}{l}(J_h + J_{ex})\left[\eta\dot{\xi} + (\ddot{\tau}_{elbow} - \ddot{\tau}_d)\cdot\delta_F + \ddot{\theta}_d\right] + \\ \sigma\left[A(\sigma_3) - A(\sigma_1)\right] - D_u\end{array}\right\}\end{array}\right\}$$
$$= -S(t)(J_h + J_{ex})^{-1}\left\{\sigma\left[A(\sigma_3) - A(\sigma_1)\right] - D_u\right\} \quad (25)$$

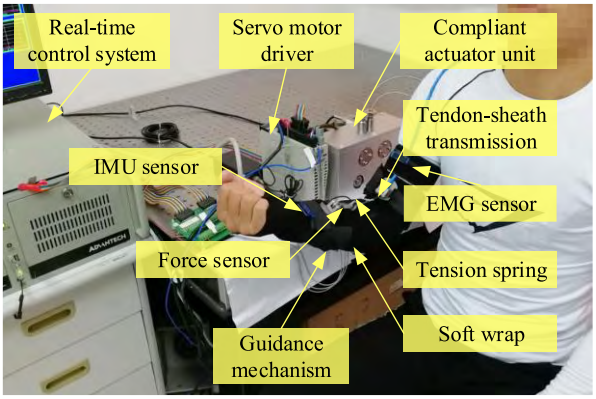

FIGURE 10. The soft exoskeleton prototype worn by a healthy subject.

$$\begin{aligned} &\leq -(J_h + J_{ex})^{-1}\sigma\,|S(t)|\,|A(\sigma_3) - A(\sigma_1)| \\ &\quad + (J_h + J_{ex})^{-1}\,|S(t)|\,|D_u| \\ &= -(J_h + J_{ex})^{-1}\,|S(t)|\,[\sigma\,|A(\sigma_3) - A(\sigma_1)| - |D_u|] \end{aligned} \tag{26}$$

Here, the lumped effects of uncertainties D_u is supposed to satisfy the following assumption:

Assumption 1: The boundary of the uncertainty term can be limited by a positive constant γ as follow [48]:

$$|D_u| < \gamma \tag{27}$$

Therefore, from (26) and (27), it can be found that if the positive constant of hitting control law σ is chosen as follow:

$$\sigma \geq \left| \frac{\gamma}{A(\sigma_3) - A(\sigma_1)} \right| \tag{28}$$

Then, inserting (27) and (28) into (26), we can get:

$$\begin{aligned} \dot{V}(t) &\leq -(J_h + J_{ex})^{-1}\,|S(t)|\,[\sigma\,|A(\sigma_3) - A(\sigma_1)| - |D_u|] \\ &\leq -(J_h + J_{ex})^{-1}\,|S(t)| \\ &\quad \times \left[\left| \frac{\gamma}{A(\sigma_3) - A(\sigma_1)} \right| \cdot |A(\sigma_3) - A(\sigma_1)| - |D_u| \right] \\ &= -(J_h + J_{ex})^{-1}\,|S(t)|\,[\gamma - |D_u|] \\ &\leq 0 \end{aligned} \tag{29}$$

Here, we can observed that $V(t)$ is positive definite, while $\dot{V}(t)$ is negative definite. Moreover, when $S(t)$ tends to infinity, $V(t)$ also approaches to infinity. Thus, the proposed controller satisfies the Lyapunov stability criteria. The proposed FSMCA control strategy is globally asymptotically stable even when the system uncertainties occur. The admittance error ξ will gradually converge to zero and approach the sliding surface (i.e., $S(t) = 0$) in finite time.

IV. EXPERIMENTS AND RESULTS

Upon completing the mechanical hardware design, dynamic modeling and FSMC admittance controller development, two kinds of experiments, including the patient-passive mode training experiments and the patient-active mode training experiments, were conducted to evaluate the effectiveness of the proposed soft exoskeleton system and control algorithm, as shown in Fig 10. The servo driving motor was set to run in torque control mode, and it can provide assistive forces to the human elbow based on the executed control algorithm and feedback sensing signals. Three healthy neurologically intact subjects with different anthropometric parameters (H1: male, weight/62 kg, height/1.72 m; H2: male, weight/70 kg, height/1.83 m, H3: female, weight/51 kg, height/1.62 m) participated in this research and provided consent before experiments. The implemented experimental protocols have been approved by the Institutional Review Board at the Nanjing University of Aeronautics and Astronautics.

A. PATIENT-PASSIVE MODE TRAINING EXPERIMENTS

The passive-mode training experiments have been divided into four different sub-experiments. More specifically, the trajectory tracking experiments without admittance regulation, the step response experiments and the frequency response experiments were carried out to validate the control performance of the inner FSMC position controller during patient-passive training, while the trajectory tracking experiments with admittance regulation were conducted to analyze the compliance of human-robot interaction with different admittance parameters. The experimenters were required to comfortably wear the rehabilitation exoskeleton and perform repetitive passive training on right elbow without active participation. The experimental results of the FSMCA controller were compared to those of a cascaded proportional-integral-derivative (CPID) controller [49] and a conventional sliding mode controller (SMC) with a proportional-integral-derivative (PID) sliding surface [50].

1) TRAJECTORY TRACKING EXPERIMENTS

According to the overall block diagram of the proposed control strategy shown in Fig. 9, the inner FSMC controller is in charge of regulating the exoskeleton configuration according to the predefined training trajectory and the value of elbow angle regulation that is output from admittance filter. Actually, the FSMC-based admittance controller can be converted into a position controller to track the predefined training trajectory, if the admittance parameters are all set to infinity. Therefore, the trajectory tracking experiments without admittance regulation (i.e., $M_d \to \infty$, $B_d \to \infty$, $K_d \to \infty$) were carried out to demonstrate the control accuracy of inner FSMC controller. The desired elbow joint trajectory was defined to follow a sinusoid wave trajectory with time-varying frequency and peak-to-peak amplitude. The first eight seconds of the desired elbow trajectory saw a frequency of 0.25 Hz and an amplitude of 90°, which then changed to 0.5 Hz and 60° from the moment $t = 8$ s to $t = 14$ s. In the last two seconds, the frequency and amplitude changed to 1 Hz and 45°, respectively. The controller parameters of CPID scheme were firstly estimated by utilizing the Ziegler and Nichols approach and then carefully optimized through trial and error [51]. The parameters of conventional SMC algorithm were optimally modulated via intensive tests to improve control accuracy and ensure system stability. The parameters of the proposed FSMCA controller were set to

TABLE 1. Statistical results of the patient-passive training experiments with different control algorithms.

Subject	Controller type	Experiment type							
		Trajectory tracking		Step response					Frequency response
		RMSE (°)	MAE (°)	Rising time (s)	5% setting time (s)	Overshoot (%)	Overshoot of Disturbance (%)	Duration of Transient phase (s)	Bandwidth (dB)
H1	CPID	6.48	12.3	0.58	0.51	1.02	18.66	0.37	1.5
	SMC	4.41	8.56	0.24	0.28	6.15	16.21	0.29	1.9
	FSMCA	2.28	4.86	0.19	0.17	1.98	11.46	0.21	4.0
H2	CPID	7.23	13.8	0.63	0.55	0.98	19.98	0.42	1.3
	SMC	4.86	9.13	0.27	0.33	6.53	16.82	0.33	1.8
	FSMCA	2.36	4.78	0.21	0.19	1.81	11.06	0.19	3.7
H3	CPID	6.06	11.1	0.56	0.50	1.22	18.09	0.35	1.5
	SMC	4.56	7.95	0.25	0.32	5.97	16.53	0.31	2.0
	FSMCA	1.99	4.36	0.18	0.15	1.89	11.28	0.20	4.1

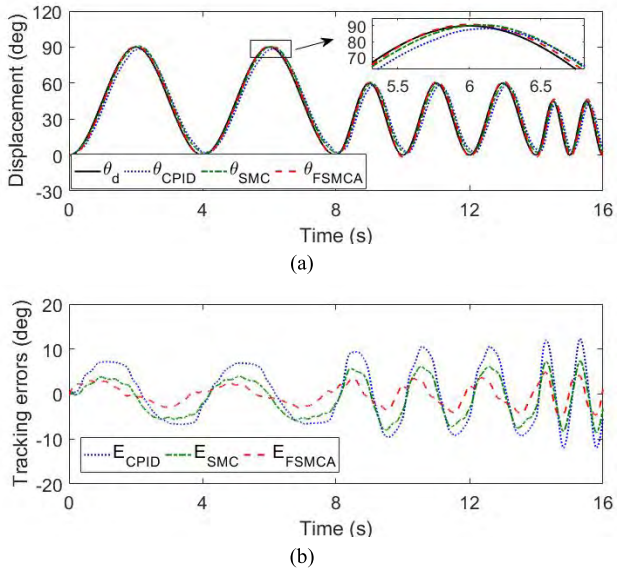

FIGURE 11. Comparison results of trajectory tracking experiments with different control strategies. (a) Comparisons between the desired trajectory and the actual trajectory; (b) Comparison of position tracking errors.

$\eta = 8.6$, $S_1 = -10.5$, $S_2 = 10.5$, $\sigma = 26.2$, $M_d = B_d = K_d = 10^{12}$.

The comparison results of trajectory tracking experiments conducted by H1 with different control strategies are shown in Fig 11. More specifically, Fig. 11(a) shows the comparisons between the desired trajectory and the actual trajectory, and Fig. 11(b) presents the histograms of position tracking errors of different control schemes. As can be found, the position control precision of the proposed FSMCA controller are better than those of the CPID controller and conventional SMC scheme, while the performance of the CPID strategy is the worst. The RMSE decline from 6.48°(CPID) and 4.41°(SMC) to 2.28°(FSMCA). Regarding the maximum absolute errors (MAE), the FSMCA algorithm obtains smallest value (i.e., 4.86°) in comparison with those of CPID algorithm (i.e., 12.3°) and conventional SMC scheme (i.e., 8.56°).

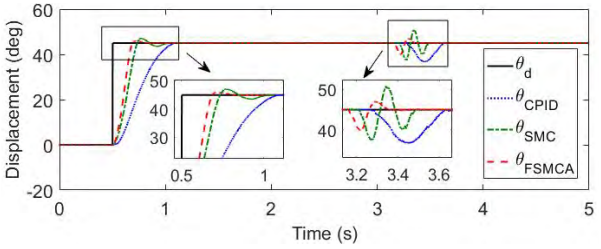

FIGURE 12. Results of step response experiments using different control strategies.

The statistical results from the trajectory tracking experiments conducted by H1, H2 and H3 are all summarized in Table 1, which demonstrates that the proposed FSMCA control algorithm is capable of guaranteeing the trajectory tracking precision in patient-passive rehabilitation training.

2) STEP RESPONSE EXPERIMENTS

To study the transient response performance of the developed FSMCA control strategy, the step response experiments were conducted using different control strategies. Moreover, in order to analyze the sensitivity of each control scheme to the outer uncertainties, an external disturbance was applied to the forearm at the time about 3 s. The step input command was defined to flex the elbow exoskeleton with a displacement of 45° at the time of 0.5 s. The control parameters of each control strategy were the same as those employed in the previous trajectory tracking experiments. The comparison results of the step response experiment conducted by H1 using different control methods are shown in Fig. 12. It can be observed that the proposed FSMCA control algorithm achieves the best step response performance and robustness. More specifically, the rising time of FSMCA controller, i.e., 0.19 s, is smaller than those of CPID controller, i.e., 0.58 s, and conventional SMC scheme, i.e., 0.24 s. Furthermore, the 5% setting time declines from 0.51 s (CPID) and 0.28 s (SMC) to 0.17 s (FSMCA) during step response experiment. Regarding to the overshoot, the FSMCA controller produces a smaller value i.e., 1.98%, in comparison with that of the conventional SMC

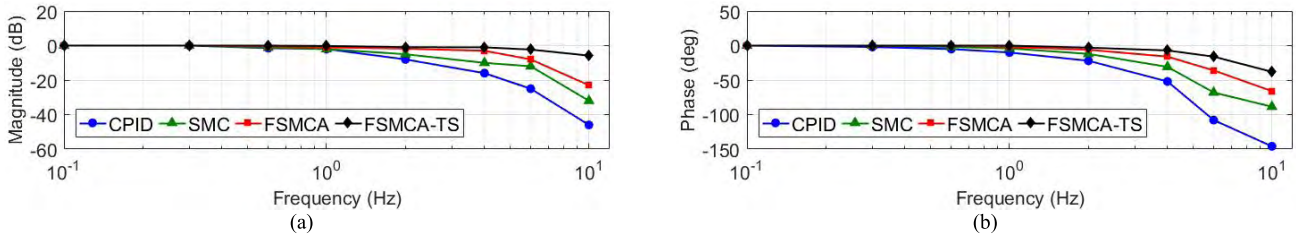

FIGURE 13. Bode diagrams of the frequency characteristics with different control strategy. (a) Magnitude characteristic; (b) Phase characteristic.

algorithm, i.e., 6.15%. The overshoot of CPID scheme is the smallest, i.e., 1.02%. In addition, the overshoot resulting from the disturbance and the duration of transient phase are about 11.46% and 0.21 s for the FSMCA scheme, which are smaller than those of CPID scheme (18.66%, 0.37 s) and SMC scheme (16.21%, 0.29 s). The statistical results from the step response experiments conducted by H1, H2 and H3 are all summarized in Table 1. Experimental results indicate that the soft exoskeleton can achieve fast response, small overshoot and strong robustness with the designed FSMCA control algorithm.

3) FREQUENCY RESPONSE EXPERIMENTS

The compliant tendon-sheath system applied in our research is capable of imitating the actuation of biological muscle-tendon tissue and providing remote compliant force transmission to the elbow exoskeleton. Nevertheless, the highly nonlinear properties of the compliant tendon-sheath transmission, such as friction, hysteresis and the compliance of tendon and springs, have negative affect on the control bandwidth of robotic system. Therefore, the sinusoid wave trajectory tracking experiments, with frequencies ranging from 0.1 Hz to 10 Hz, were carried out to further analyze and compare the closed-loop frequency properties of different control strategies. Fig. 13 describes the Bode diagram of the frequency response experiments conducted by H1. The displacement transfer characteristic of soft elbow exoskeleton is defined as the transfer relationship between the desired input trajectory references to the actual output trajectory responses during position tracking experiments.

The comparison results of the system closed-loop magnitude-frequency characteristics under different control methods are presented in Fig. 13(a). The system bandwidth reveals the frequency at which the magnitude value declines 3 dB from the low-frequency value. It can be seen that the closed-loop system bandwidth under the developed FSMCA control algorithm is about 4 Hz, which is wider than the bandwidths under CPID controller, i.e., about 1.5 Hz, and the conventional SMC control strategy, i.e., 2 Hz. Moreover, the corresponding closed-loop phase-frequency characteristics under different controllers are shown in Fig. 13(b). We can observe that, with the increase of control frequency, the phase angle of each controller decreases basically in coordination with their magnitude value. The phase angles of the designed FSMCA control algorithm decreases more slowly than the phase angles of CPID controller and conventional SMC schemes. The statistical results of the frequency response experiments conducted by H1, H2 and H3 are all summarized in Table 1.

TABLE 2. The admittance parameters of different working conditions.

Conditions	M_d (N·m·s^2/°)	B_d (N·m·s/°)	K_d (N·m·s/°)
Con1	0.20	0.20	0.20
Con2	0.10	0.10	0.10
Con3	0.06	0.06	0.06

To analyze the influences of the elastic components on frequency response characteristics, the results of CTSA are compared to those of the pure tendon-sheath actuator without tension springs. As can be found, the bandwidth of tendon-sheath actuation under FSMCA controller (FSMCA-TS) is about 8 Hz, which is wider than that of CTSA. Besides, the phase angle of CTSA decreases faster than that of tendon-sheath actuation. Thus, it can be found that the compliance feature of CTSA degrades the frequency response property of actuator. Nevertheless, since the position control bandwidth during rehabilitation training is generally limited in the range from 1 Hz to 3 Hz, the developed exoskeleton driven by CTSA and the proposed FSMCA control scheme are suitable to be utilized in the practical elbow therapeutic operation.

4) TRAJECTORY TRACKING EXPERIMENTS WITH ADMITTANCE REGULATION

The purpose of the aforementioned patient-passive training without admittance regulation is to ensure the repetitive trajectory tracking accuracy during rehabilitation training, and that is applicable to the disabled patients at the acute stage of hemiplegia and completely paralyzed without any muscle contraction. However, if parts of the motor functions of patients have been regained but still weak, the patient-passive training with admittance regulation contributes to enhancing the compliance and comfort of human-robot interaction and protecting the patients from excessive traction forces. Moreover, the actual training trajectory can be adjusted by the patients based on the interaction forces measured by force sensors. In order to analyze the control performance of the proposed FSMCA strategy with admittance regulation, the experimenter H1 was required to passively conduct the trajectory tracking experiments with three groups of different

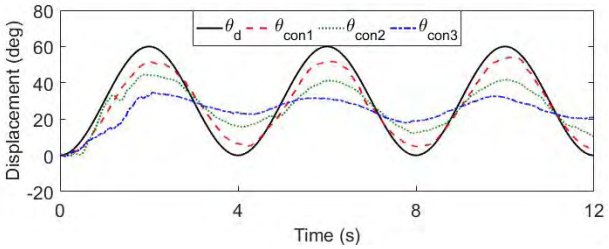

FIGURE 14. Trajectory tracking experiments with different admittance parameters.

admittance parameters, as shown in Table 2. In this case, the exoskeleton was commanded to follow a sinusoid wave trajectory with a frequency of 0.25 Hz and amplitude of 60°. The experimental results with different admittance filters are shown comparatively in Fig. 14. The RMSE under Condition1 is 6.68°, meanwhile the RMSE under Condition2 and Condition3 are 12.6° and 18.9°, respectively. The experimental results indicate that the deviation between the desired training trajectory and actual training trajectory tends to increase with the decrease of admittance parameters. By modulating the admittance parameters of the developed FSMCA controller, the system compliance of the rehabilitation robot can be changed to satisfy the passive-training requirement of patients with different weakness levels.

B. PATIENT-ACTIVE MODE TRAINING EXPERIMENTS

The major shortcoming of the patient-passive mode training is that the motion intentions of patients cannot be integrated into the treatment. Clinical therapy experience indicates that, for the patients with hemiplegia at recovery stage, the rehabilitation training combined with the active participation of patients facilitates to accelerate the regain of motor ability. The patient-active mode training experiments were conducted by different subjects to evaluate the feasibility of proposed FSMCA control strategy in free arm operation training, which can effectively induce the voluntary efforts and participations of patients during rehabilitation training. In this experiment, the motion intention were detected by the pulling forces from the distal ends of flexion tendon and extension tendon. The proposed FSMCA controller can modulate the configuration of human-robot system based on the desired mechanical admittance characteristic and the real-time interaction torque calculated from (8). The desired training position was defined to flex the elbow rehabilitation exoskeleton with a constant displacement of 45°. During the experimenters, all the subjects were commanded to actively perform reciprocating elbow flexion/extension movement on the sagittal plane with different admittance parameters. The position deviations were generally limited within the range of 0° to 90°. The relation between the interaction torque and position deviation presents the difficulty and intensity during patient-active training.

Three groups of different parameters were implemented to the admittance filter to research the patient-active control

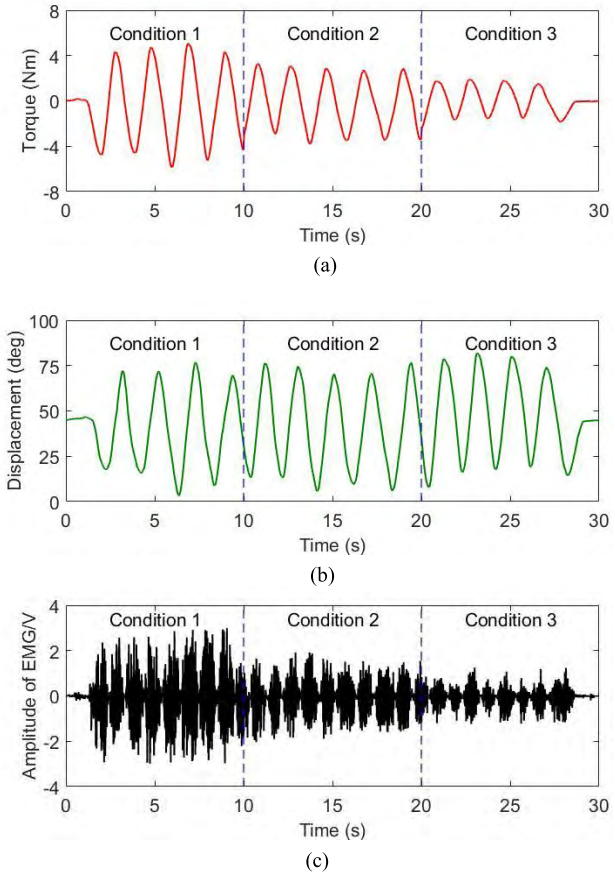

FIGURE 15. Results of patient-active training experiments conducted by the healthy subject H1 with different admittance parameters. (a) Interaction torque between human elbow and soft exoskeleton. (b) Time histories of elbow displacement. (c) Amplitude of sEMG signal from the bicipital muscle of wearer.

performance with different admittance experimental conditions, as shown in Table 2. The volunteers needed to repeat the patient-active free arm training experiment five times for each condition. The duration of each training time was set to 30 seconds. In order to analyze the impact of admittance parameters on the performance of active mode control, the training process was divided into three different phases. More specifically, the subjects were required to train with large admittance parameters (Condition1) in the first 10 seconds, which then changed to medium values (Condition2) from the moment $t = 10$ s to $t = 20$ s. Finally, the last ten seconds saw small values of admittance parameters (Condition3). According to existing research literature [52], the scale and variation of human limb muscular power can be estimated via the sEMG signals from the corresponding dominant muscles. Therefore, in the patient-active training experiments, the sEMG signals from the bicipital muscle, which dominates the elbow flexion/extension movement, were measured and analyzed to compare the training intensity with different admittance parameters.

Fig. 15 presents the results of patient-active training experiments conducted by H1 with different admittance

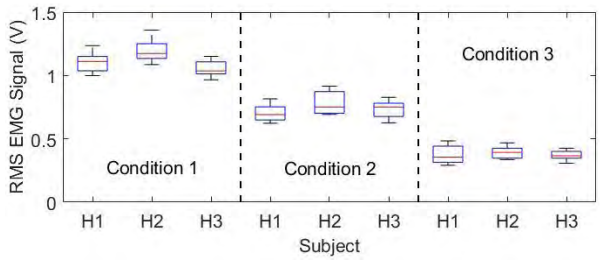

FIGURE 16. The comparison results of the RMS sEMG values of different subjects and admittance parameters.

TABLE 3. Statistical results of comparing the RMS EMG values under different experimental conditions.

Con	RMS EMG values of different subjects (V)								
	H1			H2			H3		
	Max	Min	Med	Max	Min	Med	Max	Min	Med
1	1.23	1.02	1.11	1.36	1.08	1.17	1.15	0.96	1.01
2	0.81	0.62	0.69	0.91	0.68	0.75	0.82	0.62	0.75
3	0.48	0.29	0.35	0.46	0.33	0.39	0.42	0.30	0.36

Con = condition, Max = Maximum value, Min = Minimum value, Med = median value.

parameters (single trial), including the variation of human-robot interaction torque, the time histories of elbow displacement and the corresponding amplitude of sEMG signals. As can be found, the elbow joint configuration is basically changed in accordance with the driving torque exerted by the experimenter, and that realizes the active participation of patient during rehabilitation training. Moreover, for the same free arm training task, the decrease of admittance parameters will lead to smaller interaction torque and sEMG activity. The feature of the sEMG signals shown in Fig. 15(c) is extracted by using the root mean square (RMS) method. As a result, the RMS sEMG value under the first experimental condition is about 1.12 V, and that is larger than those under the second condition, i.e, 0.73 V, and the third condition, i.e, 0.38 V. Besides, the overall experimental results of different subjects and admittance parameters in six trials are summarized and shown in Fig. 16 and Table 3. It can be clearly found that the active-training intensity can be qualitatively adjusted by changing the admittance filter of the proposed FSMCA controller, and the amplitude of sEMG signals vary from trial to trial and person to person in the same experiment. In addition, the patient-active experiments were also carried out using the tendon-sheath actuator without elastic elements, and the results indicates that the proposed CTSA system can effectively enhance the comfort, compliance and interaction coordination of rehabilitation training. Thus, the experimental results of free arm training demonstrate that the developed FSMCA algorithm is capable of providing efficient patient-active rehabilitation therapy with different motion resistance and training intensity. In practical rehabilitation training application, the admittance filter should be rationally adjusted to satisfy the capabilities and requirements of different patients.

V. CONCLUSION

In this paper, the major contributions are the design of a wearable soft elbow exoskeleton driven by the novelty CTSA system, and the development of a FSMCA control strategy that can realize patient-passive and patient-active training with different interaction compliance and training intensity. The major hardware of the soft therapeutic robot and the CTSA system designed based on the Hill-based muscle-tendon model were introduced. With the aim of improving the control accuracy in patient-passive training and inducing active participation of patient in patient-active training, the FSMCA controller is developed on the basis of the dynamic model of human-robot interaction system. A fuzzy controller is integrated into the controller to mitigate the undesirable chattering problem and ensure the asymptotic stability of closed-loop system using Lyapunov stability theory. Two kinds of experiments, including passive training experiments and active training experiments, were conducted by three healthy subjects to evaluate the control performance of the developed exoskeleton and control algorithm. Experimental results show that the FSMCA scheme can achieve higher position control precision, stronger robustness, and better frequency response characteristic when compared with the conventional CPID and SMC methods. The human-robot interaction compliance and training intensity of rehabilitation training are directly affected by the admittance parameters.

Future works will be focused on the structure optimization of soft exoskeleton for better comfort and simpler wearing procedure. Besides, the improvement strategy of controller parameters for better training effectiveness will be researched. The human-robot dynamic model will be optimized by taking the soft features of muscle tissue and straps into account. The soft exoskeleton for shoulder and wrist rehabilitation will be designed and combined with the elbow exoskeleton prototype to realize completed upper limb training.

REFERENCES

[1] N. Jackson *et al.*, "Reflections on 50 years of neuroscience nursing: The growth of stroke nursing," *J. Neurosci. Nursing*, vol. 50, no. 4, pp. 188–192, 2018.

[2] Q. Wu, X. Wang, B. Chen, and H. Wu, "Development of an RBFN-based neural-fuzzy adaptive control strategy for an upper limb rehabilitation exoskeleton," *Mechatronics*, vol. 53, pp. 85–94, Aug. 2018.

[3] A. J. Young and D. P. Ferris, "State of the art and future directions for lower limb robotic exoskeletons," *IEEE Trans. Neural Syst. Rehabil. Eng.*, vol. 25, no. 2, pp. 171–182, Feb. 2017.

[4] A. Otten, C. Voort, A. Stienen, R. Aarts, E. van Asseldonk, and H. van der Kooij, "LIMPACT: A hydraulically powered self-aligning upper limb exoskeleton," *IEEE/ASME Trans. Mechatronics*, vol. 20, no. 5, pp. 2285–2298, Oct. 2015.

[5] U. Keller, H. J. A. van Hedel, V. Klamroth-Marganska, and R. Riener, "ChARMin: The first actuated exoskeleton robot for pediatric arm rehabilitation," *IEEE/ASME Trans. Mechatronics*, vol. 21, no. 5, pp. 2201–2213, Oct. 2016.

[6] B. Brahim, M. Saad, C. Ochoa-Luna, M. H. Rahman, and A. Brahmi, "Adaptive tracking control of an exoskeleton robot with uncertain dynamics based on estimated time-delay control," *IEEE/ASME Trans. Mechatronics*, vol. 23, no. 20, pp. 575–585, Apr. 2018.

[7] J. Huang, X. Tu, and J. He, "Design and evaluation of the RUPERT wearable upper extremity exoskeleton robot for clinical and in-home therapies," *IEEE Trans. Syst., Man, Cybern., Syst.*, vol. 46, no. 7, pp. 926–935, Jul. 2016.

[8] R. R. Conti, E. Meli, and A. Ridolfi, "A novel kinematic architecture for portable hand exoskeletons," *Mechatronics*, vol. 35, pp. 192–207, May 2016.

[9] A. Riani, T. Madani, A. Benallegue, and K. Djouani, "Adaptive integral terminal sliding mode control for upper-limb rehabilitation exoskeleton," *Control Eng. Pract.*, vol. 75, pp. 108–117, Jun. 2018.

[10] W. Wu *et al.*, "Modulation of shoulder muscle and joint function using a powered upper-limb exoskeleton," *J. Biomechanics*, vol. 72, pp. 7–16, Apr. 2018.

[11] Q. Wu, X. Wang, and F. Du, "Development and analysis of a gravity-balanced exoskeleton for active rehabilitation training of upper limb," *Proc. Inst. Mech. Eng., C, J. Mech. Eng. Sci.*, vol. 230, no. 20, pp. 3777–3790, 2016.

[12] N. Vitiello *et al.*, "Functional design of a powered elbow orthosis toward its clinical employment," *IEEE/ASME Trans. Mechatronics*, vol. 21, no. 4, pp. 1880–1891, Aug. 2016.

[13] D. Buongiorno, E. Sotgiu, D. Leonardis, S. Marcheschi, M. Solazzi, and A. Frisoli, "WRES: A novel 3 DoF WRist ExoSkeleton with tendon-driven differential transmission for neuro-rehabilitation and teleoperation," *IEEE Robot. Autom. Lett.*, vol. 3, no. 3, pp. 2152–2159, Jul. 2018.

[14] X. Cui, W. Chen, X. Jin, and S. K. Agrawal, "Design of a 7-DOF cable-driven arm exoskeleton (CAREX-7) and a controller for dexterous motion training or assistance," *IEEE/ASME Trans. Mechatronics*, vol. 22, no. 1, pp. 161–172, Feb. 2017.

[15] F. Xiao *et al.*, "Design and evaluation of a 7-DOF cable-driven upper limb exoskeleton," *J. Mech. Sci. Technol.*, vol. 32, no. 2, pp. 855–864, 2018.

[16] A. T. Asbeck, K. Schmidt, and C. J. Walsh, "Soft exosuit for hip assistance," *Robot. Auton. Syst.*, vol. 73, pp. 102–110, Nov. 2014.

[17] A. U. Pehlivan, D. P. Losey, and M. K. O'Malley, "Minimal assist-as-needed controller for upper limb robotic rehabilitation," *IEEE Trans. Robot.*, vol. 32, no. 11, pp. 113–124, Feb. 2016.

[18] T. Nef, M. Guidali, and R. Riener, "ARMin III—Arm therapy exoskeleton with an ergonomic shoulder actuation," *Appl. Bionics Biomechanics*, vol. 6, no. 2, pp. 127–142, 2009.

[19] Q. Wu, X. Wang, B. Chen, and H. Wu, "Development of a minimal-intervention-based admittance control strategy for upper extremity rehabilitation exoskeleton," *IEEE Trans. Syst., Man, Cybern. B. Cybern.*, vol. 48, no. 6, pp. 1005–1016, Jun. 2018.

[20] H.-C. Hsieh, D.-F. Chen, L. Chien, and C.-C. Lan, "Design of a parallel actuated exoskeleton for adaptive and safe robotic shoulder rehabilitation," *IEEE/ASME Trans. Mechatronics*, vol. 22, no. 5, pp. 2034–2045, Oct. 2017.

[21] N. Vitiello *et al.*, "NEUROExos: A powered elbow exoskeleton for physical rehabilitation," *IEEE Trans. Robot.*, vol. 29, no. 1, pp. 220–235, Feb. 2013.

[22] Y. L. Park *et al.*, "Design and control of a bio-inspired soft wearable robotic device for ankle-foot rehabilitation," *Bioinspiration Biomimetics*, vol. 9, no. 1, p. 016007, 2014.

[23] Y. Ding, M. Kim, S. Kuindersma, and C. J. Walsh, "Human-in-the-loop optimization of hip assistance with a soft exosuit during walking," *Sci. Robot.*, vol. 3, no. 15, p. eaar5438, 2018.

[24] S. Mohammed *et al.*, "Wearable robotics for motion assistance and rehabilitation [TC spotlight]," *IEEE Robot. Autom. Mag.*, vol. 25, no. 1, pp. 19–28, Mar. 2018.

[25] B. T. Quinlivan *et al.*, "Assistance magnitude versus metabolic cost reductions for a tethered multiarticular soft exosuit," *Sci. Robot.*, vol. 2, no. 2, p. eaah4416, 2017.

[26] C. T. O'Neill, N. S. Phipps, L. Cappello, S. Paganoni, and C. J. Walsh, "A soft wearable robot for the shoulder: Design, characterization, and preliminary testing," in *Proc. IEEE Int. Conf. Rehabil. Robot. (ICORR)*, Jul. 2017, pp. 1672–1678.

[27] C. Rognon, S. Mintchev, F. Dell'Agnola, A. Cherpillod, D. Atienza, and D. Floreano, "Agnola, "FlyJacket: An upper body soft exoskeleton for immersive drone control," *IEEE Robot. Autom. Lett.*, vol. 3, no. 3, pp. 2362–2369, Jul. 2018.

[28] D. Copaci *et al.*, "New design of a soft robotics wearable elbow exoskeleton based on shape memory alloy wire actuators," *Appl. Bionics Biomechanics*, vol. 2017, Sep. 2017, Art. no. 1605101.

[29] X. Lu, F. Du, X. Wang, S. Jia, and F. Xu, "Development and fuzzy sliding mode compensation control of a power assist lower extremity exoskeleton," *Mechanics*, vol. 24, no. 1, pp. 92–99, 2018.

[30] Z. Chen, Z. Li, and C. L. P. Chen, "Disturbance observer-based fuzzy control of uncertain MIMO mechanical systems with input nonlinearities and its application to robotic exoskeleton," *IEEE Trans. Cybern.*, vol. 47, no. 4, pp. 984–994, Apr. 2017.

[31] X. Jin, S. Zhu, X. Zhu, Q. Chen, and X. Zhang, "Single-input adaptive fuzzy sliding mode control of the lower extremity exoskeleton based on human–robot interaction," *Adv. Mech. Eng.*, vol. 9, no. 2, pp. 1–9, 2017.

[32] Z. Li, C.-Y. Su, L. Wang, Z. Chen, and T. Chai, "Nonlinear disturbance observer-based control design for a robotic exoskeleton incorporating fuzzy approximation," *IEEE Trans. Ind. Electron.*, vol. 62, no. 9, pp. 5763–5775, Sep. 2015.

[33] Z. Li, B. Wang, F. Sun, C. Yang, Q. Xie, and W. Zhang, "SEMG-based joint force control for an upper-limb power-assist exoskeleton robot," *IEEE J. Biomed. Health Informat.*, vol. 18, no. 3, pp. 1043–1050, May 2014.

[34] T. Teramae, T. Noda, and J. Morimoto, "EMG-based model predictive control for physical human–robot interaction: Application for assist-as-needed control," *IEEE Robot. Autom. Lett.*, vol. 3, no. 1, pp. 210–217, Jan. 2017.

[35] K. Kiguchi and Y. Hayashi, "An EMG-based control for an upper-limb power-assist exoskeleton robot," *IEEE Trans. Syst., Man, Cybern. B, Cybern.*, vol. 42, no. 4, pp. 1064–1071, Aug. 2012.

[36] N. A. Bhagat *et al.*, "Design and Optimization of an eeg-based brain machine interface (BMI) to an upper-limb exoskeleton for stroke survivors," *Frontiers Neurosci.*, vol. 10, no. 564, p. 122, Mar. 2016.

[37] S. Crea *et al.*, "Feasibility and safety of shared EEG/EOG and vision-guided autonomous whole-arm exoskeleton control to perform activities of daily living," *Sci. Rep.*, vol. 8, Jul. 2018, Art. no. 10823.

[38] Q. Wu, X. Wang, L. Chen, and F. Du, "Transmission model and compensation control of double-tendon-sheath actuation system," *IEEE Trans. Ind. Electron.*, vol. 62, no. 3, pp. 1599–1609, Mar. 2015.

[39] L. Chen, X. Wang, J. Lu, and W. L. Xu, "Inverse transmission model and compensation control of a single-tendon–sheath actuator," *IEEE Trans. Ind. Electron.*, vol. 61, no. 3, pp. 1424–1433, Mar. 2014.

[40] A. Falisse, S. Van Rossom, I. Jonkers, and F. De Groote, "EMG-driven optimal estimation of subject-SPECIFIC hill model muscle–tendon parameters of the knee joint actuators," *IEEE Trans. Biomed. Eng.*, vol. 64, no. 9, pp. 2253–2262, Sep. 2017.

[41] A. J. van den Bogert, D. Blana, and D. Heinrich, "Implicit methods for efficient musculoskeletal simulation and optimal control," *Procedia IUTAM*, vol. 2, pp. 297–316, Jan. 2011.

[42] D. Winter, "Anthropometry," in *Biomechanics and Motor Control of Human Movement*, 4th ed. New York, NY, USA: Wiley, 2009, pp. 83–106.

[43] S. Mefoued, S. Mohammed, and Y. Amirat, "Toward movement restoration of knee joint using robust control of powered orthosis," *IEEE Trans. Control Syst. Technol.*, vol. 21, no. 6, pp. 2156–2168, Nov. 2013.

[44] D. Ao, R. Song, and J. Gao, "Movement performance of human–robot cooperation control based on EMG-driven hill-type and proportional models for an ankle power-assist exoskeleton robot," *IEEE Trans. Neural Syst. Rehabil. Eng.*, vol. 25, no. 8, pp. 1125–1134, Aug. 2017.

[45] T. Proietti, V. Crocher, A. Roby-Brami, and N. Jarrassé, "Upper-limb robotic exoskeletons for neurorehabilitation: A review on control strategies," *IEEE Rev. Biomed. Eng.*, vol. 9, pp. 4–14, 2016.

[46] L. A. Tuan, Y. H. Joo, P. X. Duong, and L. Q. Tien, "Parameter estimator integrated-sliding mode control of dual arm robots," *Int. J. Control, Automat. Syst.*, vol. 15, no. 6, pp. 2754–2763, 2017.

[47] E. Pourjavad and R. V. Mayorga, "A comparative study and measuring performance of manufacturing systems with Mamdani fuzzy inference system," *J. Intell. Manuf.*, pp. 1–13, Feb. 2017, doi: 10.1007/s10845-017-1307-5.

[48] A. F. Amer, E. A. Sallam, and W. M. Elawady, "Adaptive fuzzy sliding mode control using supervisory fuzzy control for 3 DOF planar robot manipulators," *Appl. Soft Comput.*, vol. 11, no. 8, pp. 4943–4953, 2011.

[49] Q. C. Wu *et al.*, "Design and control of a powered hip exoskeleton for walking assistance," *Int. J. Adv. Robotic Syst.*, vol. 12, no. 3, p. 18, 2015.

[50] Q. Wu, X. Wang, F. Du, and R. Xi, "Modeling and position control of a therapeutic exoskeleton targeting upper extremity rehabilitation," *Proc. Inst. Mech. Eng., C, J. Mech. Eng. Sci.*, vol. 231, no. 23, pp. 4360–4373, 2017.

[51] A. Zolotas, F. Hassan, and T. Smith, "Optimized Ziegler-Nichols based PID control design for tilt suspensions," *J. Eng. Sci. Technol. Rev.*, vol. 10, no. 5, pp. 17–24, 2017.
[52] X. Chen, Y. Zeng, and Y. Yin, "Improving the transparency of an exoskeleton knee joint based on the understanding of motor intent using energy kernel method of EMG," *IEEE Trans. Neural Syst. Rehabil. Eng.*, vol. 25, no. 6, pp. 577–588, Jun. 2017.

QINGCONG WU received the B.S. and Ph.D. degrees in mechatronics engineering from Southeast University, Nanjing, China, in 2011 and 2016, respectively. He is currently an Assistant Professor with the College of Mechanical and Electrical Engineering, Nanjing University of Aeronautics and Astronautics, Nanjing, China. His research interests include robotics, human–robot interaction control, tendon-sheath transmission theory, gravity balancing theory, and the application of exoskeleton to neuromuscular rehabilitation.

XINGSONG WANG received the B.S. and M.S. degrees from Zhejiang University, Hangzhou, China, in 1988 and 1991, respectively, and the Ph.D. degree from Southeast University, Nanjing, China, in 2000, all in mechanical engineering. He was a Visiting Scientist with the School of Mechanical Engineering, Concordia University, Canada, from 2000 to 2002 and with the School of Mechanical Engineering, Purdue University, USA, from 2007 to 2008. He is currently a Full Professor with the School of Mechanical Engineering and the Head of the Department of Mechatronics, Southeast University. His current research interests include control theory with application in precision CNC machine tools, advanced mechatronics with applications in biomedical engineering, tendon-sheath transmission theory with application in rescue robots, and Mecanum-wheels-based AGV systems designing.

BAI CHEN received the B.S. and Ph.D. degrees in mechanical engineering from Zhejiang University, Hangzhou, China, in 2000 and 2005, respectively. He is currently a Full Professor with the College of Mechanical and Electrical Engineering, Nanjing University of Aeronautics and Astronautics. His current research interests include minimally invasive neurosurgery robot, virtual surgery system, force feedback control, and interventional therapy.

HONGTAO WU received the B.S. degree from Yanshan University, Hebei, China, in 1982, and the M.S. and Ph.D. degrees from Tianjin University, Tianjin, China, in 1985 and 1992, respectively, all in mechanical engineering. He is currently a Full Professor with the College of Mechanical and Electrical Engineering, Nanjing University of Aeronautics and Astronautics. His current research interests include parallel robot, robot kinematics, and multibody system dynamics.